Japanese Journal of Applied Physics

REGULAR PAPER

Enhanced contact properties of $MoTe_2$-FET via laser-induced heavy doping

To cite this article: Tianshun Xie *et al* 2023 *Jpn. J. Appl. Phys.* **62** SC1010

Japanese Journal of Applied Physics **62**, SC1010 (2023) **REGULAR PAPER**
https://doi.org/**10.35848/1347-4065/aca67e**

Enhanced contact properties of $MoTe_2$-FET via laser-induced heavy doping

Tianshun Xie[1*], Kazuki Fukuda[1], Mengnan Ke[1], Peter Krüger[1], Keiji Ueno[2], Gil-Ho Kim[3], and Nobuyuki Aoki[1*]

[1]*Department of Materials Science, Chiba University, Chiba 263-8255, Japan*
[2]*Department of Chemistry, Saitama University, Saitama 338-8570, Japan*
[3]*School of Electronic and Electrical Engineering and Sungkyunkwan Advanced Institute of Nanotechnology (SAINT), Sungkyunkwan University, Suwon 16419, Republic of Korea*

[*]E-mail: xietianshun@chiba-u.jp; n-aoki@faculty.chiba-u.jp

Received October 20, 2022; revised November 23, 2022; accepted November 27, 2022; published online December 23, 2022

The doping technique is vital for applying two-dimensional (2D) materials such as transition metal dichalcogenide (TMDC)-based field effect transistors (FETs), which can control the channel polarity and improve the performance. However, as conventional doping techniques for silicon-based FET are not suitable for 2D materials, the realization of heavy doping of TMDC materials is challenging, especially for n-type heavy doping. This study reports a simple, regioselective, controllable, and chemically stable heavy doping method for 2H-$MoTe_2$ crystal via high-density laser irradiation. The polarity of the doping can be controlled by changing the irradiation environment. For the $MoTe_2$-nFET, good performance with enhanced contact properties was obtained using the contact doping method via laser irradiation in a vacuum environment.

1. Introduction

Traditional Si-based metal oxide semiconductor field effect transistors (MOSFETs) contain many dangling-bond-induced traps and exhibit short-channel effects in the post-Moore era, making it more challenging to continue Moore's Law.[1)] Transition metal dichalcogenide (TMDC) semiconductors, which comprise one transition metal atom and two chalcogen atoms, have an adjustable bandgap of 1–2 eV by selecting the elements and are chemically stable.[2–4)] A two-dimensional (2D) transistor can effectively prevent the short-channel effect and it has become the best candidate to replace silicon in next-generation integrated circuits.[5)] 2H-$MoTe_2$ is a member of the TMDC family as a semiconductor with a small band gap of 1.1 eV in monolayer and 0.88 eV in multilayer.[6–8)] Intrinsic 2H-$MoTe_2$ always shows ambipolar transfer properties due to its small band gap and can be easily doped to exhibit n- or p-type transfer properties.[9–12)] Therefore, it has excellent potential for applications in complementary MOSFET.[13–15)] However, the 2D-FET using TMDC materials still presents a significant challenge in contact properties owing to the Fermi level pinning (FLP) effect in the contact interface caused by intrinsic defects and metal deposition.[16–20)] Therefore, it is difficult to control the channel polarity of the device by selecting a contact metal. Many previous studies have been conducted to improve contact properties. For example, de-pinning interfaces are fabricated by inserting an insulating layer such as monolayer h-BN or Al_2O_3 between metal and 2H-$MoTe_2$.[14,21)] Moreover, using a semi-metallic polymorphic structure such as 1 T′-$MoTe_2$ as an electrode instead of a metal contact with 2H-$MoTe_2$ and it shows a low contact resistance and ohmic carrier injunction.[22–24)] Unlike these methods, contact doping is also an excellent way to decrease contact resistance by reducing the depletion width. However, traditional heavy doping methods, such as ion implantation, are significantly challenging to apply to TMDC materials because of the severe damage caused to the crystal and thermal repairing is not applicable. Chemical doping is a promising method for TMDC materials; however, its doping concentration is usually low.[25)] So far, it has only been used to dope the carrier to change the polarity of the device and improve its performance.[26)] Although there is a report on chemically heavy n-type doping of 2H-$MoTe_2$ crystal using a benzyl viologen solution, this doping method is not regioselective and unsuitable for large-scale integrated circuits.[27)] Recently, several studies have reported using ozone by UV irradiation to form a WO_x layer having a high work function on the surface of WSe_2, which absorbs electrons from the under-layer and thus heavily dopes the crystalline in p-type by the charge transfer mechanism.[28,29)] However, this method is unstable, and regioselective doping is difficult. In addition, the technique is suitable only for p-type doping, and whether the WO_x layer participates in the conduction has not been clarified yet. For applying laser irradiation on $MoTe_2$-FET, it has been reported that weak laser irradiation in an atmosphere environment is a good method for p-type doping.[30)] Other studies have used laser irradiation to make the irradiated region undergo a phase transition, which changes the structure from 2H to 1 T′, and the laser-induced 1 T′-$MoTe_2$ can form good contact with 2H-$MoTe_2$.[31,32)] However, there have been no reports on the quantitative estimation of the barrier height and the contact resistance by using heavy contact doping via laser irradiation. In this study, a regioselective heavy doping method for 2H-$MoTe_2$ via high-density laser irradiation was reported. In addition, heavy n- or p-type doping can be achieved by changing the environment in which the sample is placed. Thus, a tunneling-FET (TFET) using $MoTe_2$ can be realized by laser irradiation in different environmental conditions. Some experimental results on TFET devices fabricated by this technique have been presented at the 2022 International Conference on Solid State Devices and Materials (SSDM 2022).[33)] Herein, we analyzed the principle of laser-induced doping in detail and demonstrated that the contact properties of the $MoTe_2$-nFET were significantly improved via the heavy n-type doping by high-density laser irradiation in a vacuum environment.

2. Experimental methods

The 2H-$MoTe_2$ bulk crystal was purchased from HQ Graphene, and multilayer 2H-$MoTe_2$ crystals were exfoliated with a blue tap on a 300 nm SiO_2-coated p^{++}-Si substrate. The thickness of the 2H-$MoTe_2$ crystals used in this study

was about 15 nm. Electrodes were fabricated using electron beam lithography and electron beam metal deposition. 2H-$MoTe_2$ was placed on the prefabricated electrodes via a dry transfer process for the bottom contact sample. Laser irradiation was performed using a continuous wave laser with a wavelength of 532 nm and an output power of 1 W. The laser is guided into a vacuum chamber through an optical microscope. Since a 20× objective lens was used to focus the laser, the laser spot was 4 μm in diameter on a sample surface. The power of the laser used to irradiate the 2H-$MoTe_2$ crystal in the chamber was over 100 mW; thus, the optical power density was over 0.8 MW cm^{-2}. The time for each laser irradiation was 1 s. Raman spectra were measured using a JASCO RPM-510 Raman Spectrometer with an excitation wavelength of 532 nm installed in an Olympus BX-51 optical microscope. For the contact-doped $MoTe_2$-nFET, the electrode pattern was first engraved using electron beam lithography. After development, the contact area is irradiated locally with a laser in a vacuum, causing the crystal of the contact area to be heavily n-type doped. Finally, the metal (Cr/Au) was evaporated onto the contact area. All electrical measurements were performed using a Keithley 2614 B System Source Meter in a vacuum probe station.

3. Results and discussion

3.1. Laser-induced heavy n-doping

Figure 1(a) shows a top-contacted $MoTe_2$-FET sample after laser irradiation between the electrodes in a vacuum. The laser created a hole in the $MoTe_2$ crystal at the irradiated region. The diameter of the hole is almost the same as the size of the laser spot. Raman spectroscopy was used to confirm the crystalline structure inside and in the vicinity of the hole. No signal was observed in the hole within the wave-number range, indicating no residue remained after the irradiation of the optical power density of 0.8 MW cm^{-2}. Before laser irradiation, the original sample showed two prominent peaks at 170 and 230 cm^{-1}, which correspond to the A_{1g} mode and E_{2g} mode of 2H-$MoTe_2$ as shown in Fig. 1(b). After laser irradiation, no significant change was observed in the spectrum at the regions indicated by red-dotted rectangular close to the hole. The color of the remained $MoTe_2$ crystal did not change after the irradiation as shown in Fig. 1(a), indicating that the crystal did not exhibit a layer-thinning phenomenon or phase transition caused by the influence of the laser. Figure 1(c) shows the electrical properties of the sample before and after the irradiation. The original sample showed an n-type semiconducting transfer property with an on/off ratio of 10^3. After laser irradiation in the channel, the transfer property changed to n^+-property with a high-drain current (I_d) and almost independent of the gate voltage (V_g). Figure 1(d) shows the transfer properties of the n^+-doped sample at different temperatures. The current values in each curve decreased slightly with decreasing the temperature however no significant change was observed in the shape of the curve. This result indicates that the channel region includes a gate-independent degenerately heavily doped region and a gate-dependent lightly doped one in parallel

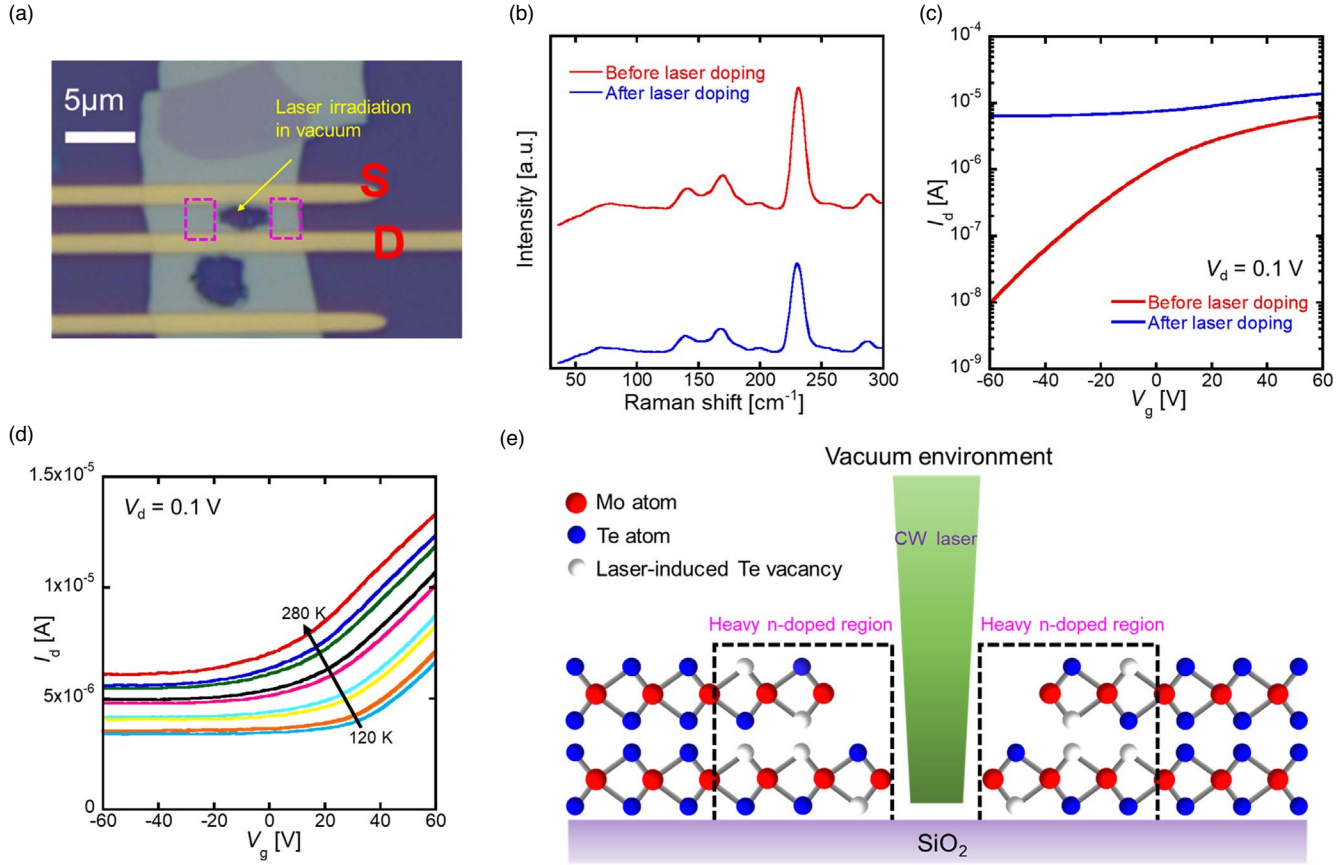

Fig. 1. (Color online) (a) Optical microscope image of the sample. (b) Raman spectroscopy of the original crystal and doped crystal. (c) Transfer properties of the $MoTe_2$-FET before and after laser doping. (d) Temperature dependence of transfer property of heavy n-type doped $MoTe_2$-FET. (e) Schematic diagram of heavy n-type doping via laser irradiation in a vacuum.

however, even the heavily doped region has a small potential barrier at the contact region.

Generally, $MoTe_2$ crystals are easily damaged by heat in the atmosphere because of the weak stability of Te atoms. Therefore, increasing the temperature above 400 K began to produce Te vacancies. It is known that such chalcogen-atom vacancies have an effect of n-type doping in TMDC crystals,[34] and also our first-principal density functional theory calculation revealed an appearance of donor level in the band gap close to the conduction band in $MoTe_2$. Owing to increasing the temperature by the irradiation of the focused laser, the $MoTe_2$ crystal absorbed the light because the energy of the green laser was larger than that of the band gap of the multilayer $MoTe_2$, 0.88 eV.[8] The temperature of the $MoTe_2$ crystal during the irradiation can be estimated as above 1200 K[35] consequently the crystal was decomposed into Mo and Te atoms and completely sublimated in a vacuum environment as schematically shown in Fig. 1(e); therefore, no Raman spectrum was observed in the hole. However, due to the Gaussian profile of the laser, the temperature of $MoTe_2$ crystal around the hole is also heated up, and then the sublimation of Te atoms creates Te vacancies. Consequently, a heavily n-doped region appears in the vicinity of the hole, and the doping level gradually decays when going away from the hole. Even when the n-doped sample was placed in the atmosphere, no change in the doping level was observed, indicating that this laser-induced heavy n-type doping is stable.

3.2. Laser-induced heavy p-doping

In order to confirm the effect of laser irradiation in the atmosphere, the $MoTe_2$-FET sample was placed in the Raman spectrometer, and the sample was irradiated linearly with a focused laser of the power density of 0.5 MW cm^{-2} by moving the sample stage. Figure 2(a) shows a bottom-contact $MoTe_2$-FET sample after laser irradiation. A hole (groove) was also created in the crystal however the irradiated region showed an evident color change, which resulted in a thinning behavior. Compared with the case of laser irradiation in a vacuum, there is often a crystal residue in a hole or groove. Raman spectroscopy was used to confirm the crystalline structure in the sample. As shown in Fig. 2(b), the directly irradiated area shows a prominent Raman peak at 120 cm^{-1}, which corresponds to the A_{1g} mode of pure Te.[35] Also, two peaks at 200 and 227 cm^{-1} correspond to the spectra of MoO_2.[36] Thus, the residuals in the hole (groove) are not layer-thinned $MoTe_2$ crystal but Te atoms and Mo oxide (MoO_2) after the thermal decomposition caused by the laser irradiation. However, the adjacent area where we focused on showed no significant change in the Raman spectrum from the original one, which corresponds to the 2H-$MoTe_2$. This indicates that no phase transition occurred in the adjacent area. Figure 2(c) shows the transfer curves of the adjacent area before and after the laser irradiation using the electrodes shown in Fig. 2(a). The curve changes from an n-type semiconducting transfer property to a heavily-doped p^+-type property. This p^+-type region showed good stability, even in a vacuum and at low temperatures as shown in Fig. 2(d). Figure 2(e) shows the schematic diagram in the case of laser irradiation in the atmospheric environment.

The important experimental fact is that the absorption of oxygen molecules at the Te vacancies for p-type doping needs a heating process; therefore, the n-doped sample prepared by laser irradiation in a vacuum does not change the polarity and the carrier density, even when the sample is exposed to oxygen at room temperature. In addition, it is known that Mo oxide acts as a suitable acceptor for TMDC crystals due to a charge transfer process. The MoO_2 included in the residue inside or around the irradiated region may play a role of an acceptor for the 2H-$MoTe_2$ in the vicinity of the hole.

3.3. Contact doping for $MoTe_2$-FET

In $MoTe_2$-FETs, top-contact using conventional metals usually causes poor contact properties by the FLP effect and severely inhibits the performance. Thus, in this study, the contact doping method via laser irradiation is applied to thin the Schottky barrier caused by the FLP effect and reduce the contact resistance. Figure 3(a) shows a schematic diagram and an optical microscope image of the contact-doped $MoTe_2$-FET. Metallic source and drain electrodes were contacted with two heavily n-doped regions prepared by laser irradiation in a vacuum before the metal deposition. This sample showed an evident n-type transfer property with a high on/off ratio of 10^4 at room temperature and 10^7 at 125 K, as shown in Fig. 3(b). The current in the on-state has negligible temperature dependence, indicating no energy barrier exists at high gate voltages. The drain current-drain voltage (I_d–V_d) curves of conventional $MoTe_2$-FETs usually show a Schottky characteristic in which the device performance is limited in a low-bias region because of the significant energy barrier in the contact interface between the metal and the $MoTe_2$. However, our sample showed good ohmic characteristics at room temperature as seen in Fig. 3(c). Moreover, even at 125 K, the sample still showed ohmic features as seen in Fig. 3(d), indicating that a suitable contact property was obtained via the contact doping technique by laser irradiation.

However, the temperature dependence of current in the low gate voltage region indicates that a certain level of energy barrier still exists at the contact interface. The Schottky barrier height and contact resistance were estimated using thermionic equations and the *Y*-function method to prove the excellent contact property further. Equations (1) and (2) describe the thermionic equations for the Schottky barrier height:[16,37]

$$I_d = WA_{2D}^{*}T^{\frac{3}{2}}\exp\left(-\frac{q\varnothing_B}{kT}\right)\left[1-\exp\left(-\frac{qV_d}{kT}\right)\right] \tag{1}$$

$$A_{2D}^{*} = \frac{q\sqrt{8\pi m^{*}k^3}}{h^2}$$

$$\varnothing_B = -\frac{k}{q}\left[\frac{\Delta In(I_d/T^{2/3})}{\Delta T^{-1}}\right], \tag{2}$$

where I_d is the drain current, W is the channel width, A_{2D}^{*} is the modified Richardson constant, k is the Boltzmann constant, q is the electrical charge, m^{*} is the effective mass, $\varnothing_B$ is the Schottky barrier height, and V_d is the applied drain voltage. Figure 4(a) shows the Schottky barrier height at various gate voltages, where the effective barrier height can be derived from the turning point of the slope of the curve corresponding to the flat band condition, which shows just

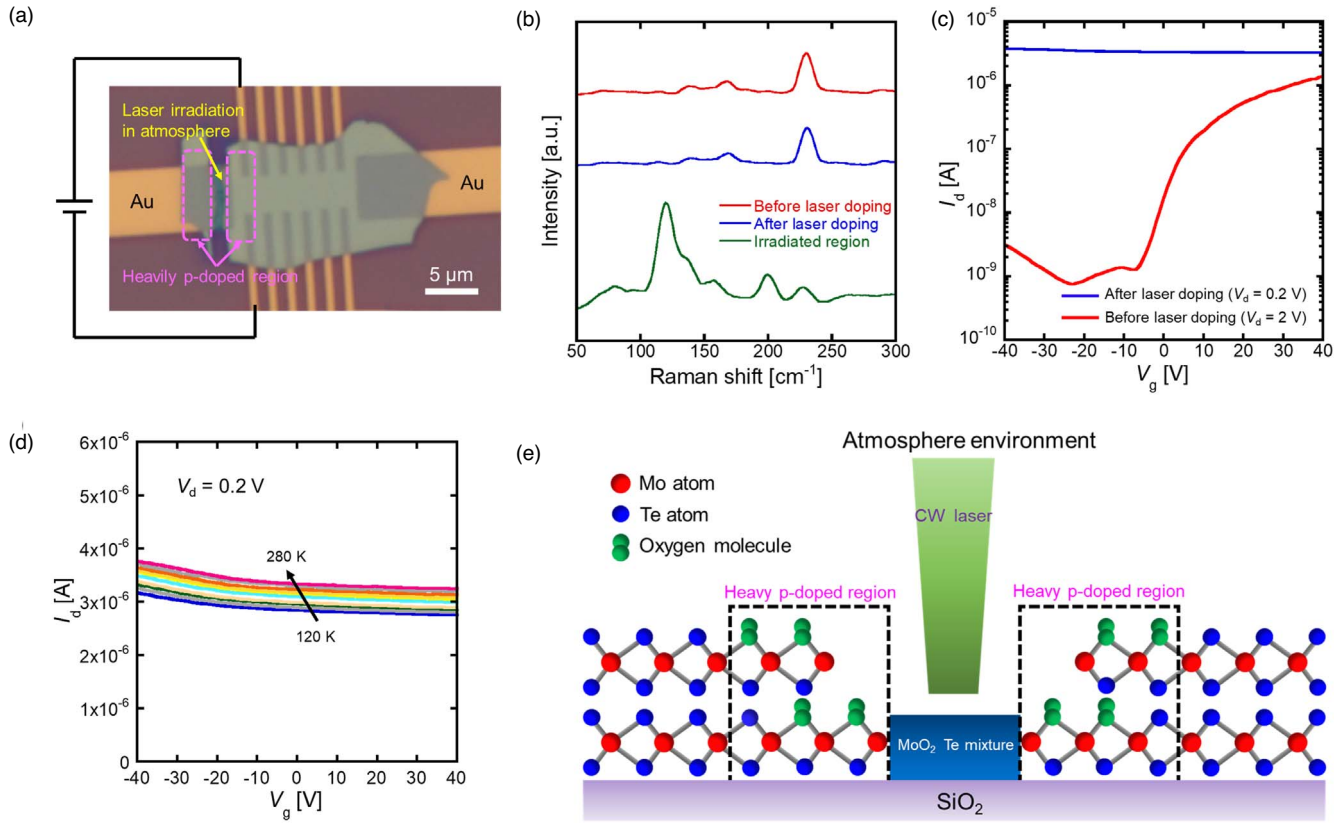

Fig. 2. (Color online) (a) Optical microscope image of the sample. (b) Raman spectroscopy of the original crystal and doped crystal. (c) Transfer properties of the $MoTe_2$-FET before and after laser doping. (d) Temperature dependence of transfer property of heavy p-type doped $MoTe_2$-FET. (e) Schematic diagram of heavy p-type doping via laser irradiation in an atmosphere.

6 meV. This indicates that the sample can exhibit good contact properties when the temperature is above 70 K. The *Y*-function method is applied following Ref. 38. The *Y*-function is defined as

$$Y = \frac{I_d}{\sqrt{g_m}} = \frac{I_d}{\sqrt{dI_d/dV_g}}, \tag{3}$$

where g_m is the transconductance defined by dI_d/dV_g. The threshold voltage (V_T) is extracted through the Y–V_g curve. Then the low-field mobility (μ_0) can be calculated as

$$Y = (V_g - V_T)\sqrt{\frac{W}{L}C_{ox}\mu_0 V_d}, \tag{4}$$

where L is the channel length, C_{ox} is the capacitance of the gate insulator. Next, the mobility attenuation factor (θ) is obtained by using the equation

$$I_d = \frac{W}{L}C_{ox}(V_g - V_T)\frac{\mu_0}{1 + \theta(V_g - V_T)} \times V_d. \tag{5}$$

Finally, the contact resistance can be calculated from the relation between θ and R_C, namely

$$\theta = \frac{W}{L}\mu_0 C_{ox} R_c. \tag{6}$$

For the contact resistance in the on-state ($V_g > 0$) at room temperature, an average value of 56 kΩ μm was obtained, as shown in Fig. 4(b). Such a small contact resistance proves that good contact properties have been achieved compared to conventional $MoTe_2$-FETs. Figure 4(c) shows the temperature dependence of the mobility at $V_g = 40$ V and then the mobility at room temperature is 22 cm^2 Vs^{-1}. If the contact properties are poor, the mobility decreases with decreasing temperature due to the high contact resistance.[39] However, the mobility of this sample increases with decreasing temperature, which indicates that the phonon scattering process in the channel is the dominant mechanism in the sample rather than the contact barrier. These experimental results prove that laser irradiation is a suitable method for contact doping to enhance the device performance of the $MoTe_2$-FET.

4. Conclusions

Heavy n-type and p-type doping of 2H-$MoTe_2$ crystal was achieved by high-density laser irradiation in a vacuum and an atmosphere environment, respectively. The $MoTe_2$-nFET showed excellent performance with a negligible Schottky contact barrier of 6 meV and low contact resistance of 56 kΩ μm at room temperature via the contact doping method by laser irradiation in a vacuum. In addition, heavy p-type doping by laser irradiation in the atmosphere can also improve the contact properties of $MoTe_2$-pFET. The heavy doping technique appears to be useful for the realization of a

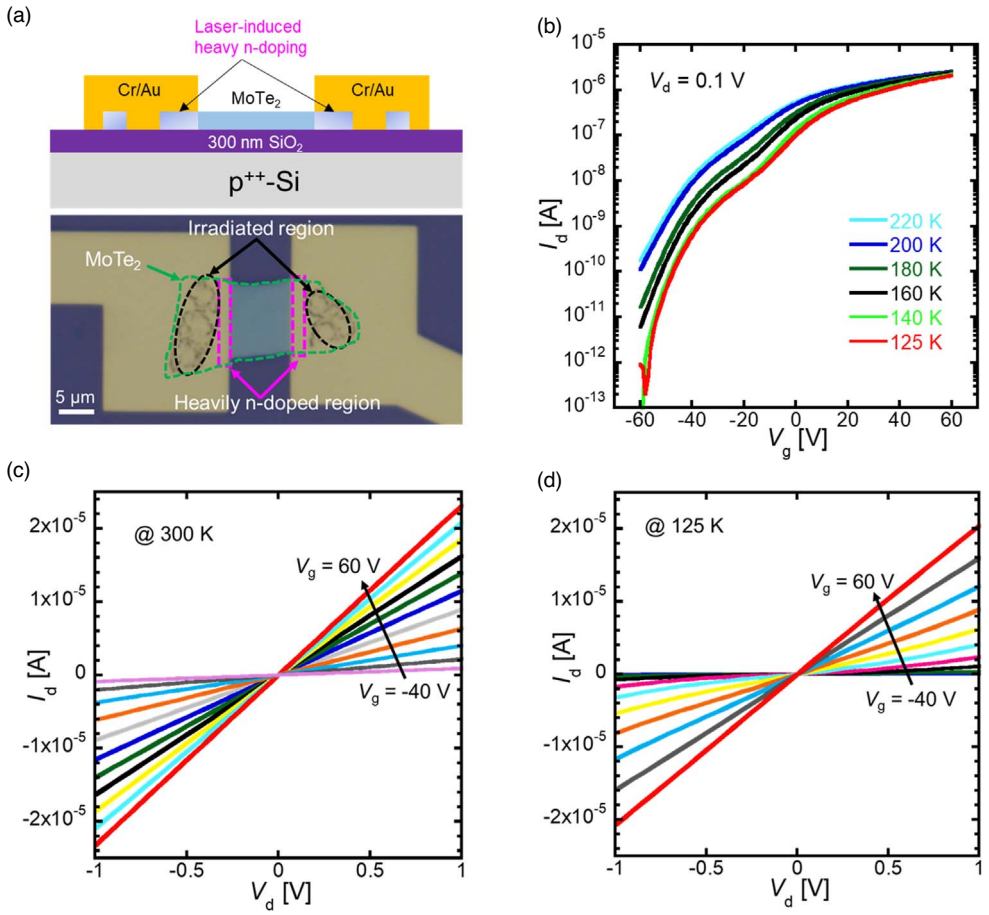

Fig. 3. (Color online) (a) Schematic diagram and optical microscope image of contact-doped $MoTe_2$-FET. (b) Transfer curves of contact-doped $MoTe_2$-FET at different temperatures. *I*–*V* curves of contact-doped $MoTe_2$-FET at (c) room temperature and (d) low temperature in V_g varied from −40 to 60 V.

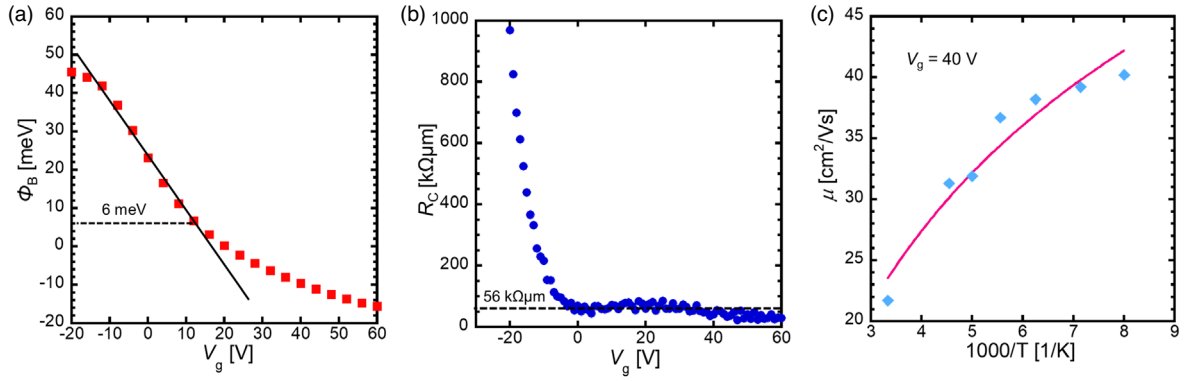

Fig. 4. (Color online) (a) Schottky barrier height of contact-doped $MoTe_2$-FET at various gate voltages. (b) Contact resistance which calculated by the *Y*-function method at various gate voltages. (c) Two terminal mobilities at different temperatures.

TFET using $MoTe_2$. However, laser-induced doping is not only suitable for $MoTe_2$ but also for other TMDC materials such as MoS_2.

Acknowledgments

T.X. was supported by JST, the establishment of university fellowships towards the creation of science technology innovation, Grant Number JPMJFS2107. T.X. was also supported by Initiative for Realizing Diversity in the Research Environment. This work was supported by the JSPS KAKENHI Grant Numbers 18H01812 and 20J20052, and Bilateral Joint Research Project between JSPS and NRF. G.-H.K. was supported under the framework of the international cooperation program managed by the National Research Foundation of Korea (Grant 2021K2A9A2A08000168). K.U. was supported by the JSPS KAKENHI Grant Numbers 18H01822 and 21K04826.

ORCID iDs

Keiji Ueno https://orcid.org/0000-0002-5535-9382

1) R. K. Ratnesh, A. Goel, G. Kaushik, H. Garg, M. Singh, and B. Prasad, Mater. Sci. Semicond. Process. **134**, 106002 (2021).
2) S. J. McDonnell and R. M. Wallace, Thin Solid Films **616**, 482 (2016).
3) H. Li, Y. Shi, M. H. Chiu, and L. J. Li, Nano Energy **18**, 293 (2015).

4) S. Das, M. Kim, J. W. Lee, and W. Choi, Crit. Rev. Solid State Mater. Sci. **39**, 231 (2014).
5) C. Song et al., ACS Nano **14**, 16266 (2020).
6) C. Ruppert, B. Aslan, and T. F. Heinz, Nano Lett. **14**, 6231 (2014).
7) I. G. Lezama, A. Arora, A. Ubaldini, C. Barreteau, E. Giannini, M. Potemski, and A. F. Morpurgo, Nano Lett. **15**, 2336 (2015).
8) I. G. Lezama, A. Ubaldini, M. Longobardi, E. Giannini, C. Renner, A. B. Kuzmenko, and A. F. Morpurgo, 2D Mater. **1**, 021002 (2014).
9) B. Zhang et al., Nanomaterials **12**, 1325 (2022).
10) T. Gao, X. Li, L. Han, and Y. Wu, 5th IEEE Electron Devices Technology & Manufacturing Conf. (EDTM), 2021, p. 1, 10.1109/EDTM50988.2021.9421022.
11) S. Kim, Y. Roh, Y. Choi, A. H. Jun, H. Seo, and B. K. Ju, Appl. Sci. **12**, 3840 (2022).
12) S. A. Ahsan, S. K. Singh, M. A. Mir, M. Perucchini, D. K. Polyushkin, T. Mueller, G. Fiori, and E. G. Marín, IEEE Trans. Electron Devices **68**, 3096 (2021).
13) J. Y. Lim, A. Pezeshki, S. Oh, J. S. Kim, Y. T. Lee, S. Yu, D. K. Hwang, G. H. Lee, H. J. Choi, and S. Im, Adv. Mater. **29**, 1701798 (2017).
14) Y. J. Park, A. K. Katiyar, A. T. Hoang, and J. H. Ahn, Small **15**, 1901772 (2019).
15) J. Chen, P. Li, J. Zhu, X. M. Wu, R. Liu, J. Wan, and T. L. Ren, IEEE Trans. Electron Devices **68**, 4748 (2021).
16) C. Kim, I. Moon, D. Lee, M. S. Choi, F. Ahmed, S. Nam, Y. Cho, H. J. Shin, S. Park, and W. J. Yoo, ACS Nano **11**, 1588 (2017).
17) C. M. Smyth, R. Addou, C. L. Hinkle, and R. M. Wallace, J. Phys. Chem. C **123**, 23919 (2019).
18) Y. Guo, D. Liu, and J. Robertson, Appl. Phys. Lett. **106**, 173106 (2015).
19) K. Sotthewes, R. Van Bremen, E. Dollekamp, T. Boulogne, K. Nowakowski, D. Kas, H. J. W. Zandvliet, and P. Bampoulis, J. Phys. Chem. C **123**, 5411 (2019).
20) X. Liu, M. S. Choi, E. Hwang, W. J. Yoo, and J. Sun, Adv. Mater. **34**, 2108425 (2022).
21) M. J. Mleczko, A. C. Yu, C. M. Smyth, V. Chen, Y. C. Shin, S. Chatterjee, Y. C. Tsai, Y. Nishi, R. M. Wallace, and E. Pop, Nano Lett. **19**, 6352 (2019).
22) S. Yang, X. Xu, W. Xu, B. Han, Z. Ding, P. Gu, P. Gao, and Y. Ye, ACS Appl. Nano Mater. **3**, 10411 (2020).
23) X. Zhang et al., ACS Appl. Mater. Interfaces **11**, 12777 (2019).
24) R. Ma et al., ACS Nano **13**, 8035 (2019).
25) M. W. Iqbal, A. Amin, M. A. Kamran, H. Ateeq, E. Elahi, G. Hussain, S. Azam, S. Aftab, T. Alharbi, and A. Majid, Superlattices Microstruct. **135**, 106247 (2019).
26) M. W. Iqbal, E. Elahi, A. Amin, G. Hussain, and S. Aftab, Superlattices Microstruct. **137**, 106350 (2020).
27) D. Qu, X. Liu, M. Huang, C. Lee, F. Ahmed, H. Kim, R. Ruoff, J. Hone, and W. Yoo,, J. Adv. Mater. **29**, 1606433 (2017).
28) S. Yang, G. Lee, and J. Kim, ACS Appl. Mater. Interfaces **13**, 955 (2020).
29) M. Yamamoto, S. Nakaharai, K. Ueno, and K. Tsukagoshi, Nano Lett. **16**, 2720 (2016).
30) J. Chen, J. Zhu, Q. Wang, J. Wan, and R. Liu, Small **16**, 2001428 (2020).
31) S. Cho et al., Science **349**, 625 (2015).
32) G. Y. Bae, J. Kim, J. Kim, S. Lee, and E. Lee, Nanomaterials **11**, 2805 (2021).
33) T. Xie, K. Fukuda, M. Ke, and N. Aoki, Ext. Abst. Solid State Devices and Materials (SSDM 2022), 2022, p. 453.
34) K. Cho et al., ACS Nano **9**, 8044 (2015).
35) K. Sakanashi et al., Nanotechnology **31**, 205205 (2020).
36) S. Camacho-Lopez, I. O. Perez-Lopez, M. Cano-Lara, A. Esparza-Garcia, M. C. Maya-Sanchez, J. A. Reynoso-Hernandez, and M. Camacho-Lopez, Phys. Status Solidi **215**, 1800226 (2018).
37) S. B. Mitta, M. S. Choi, A. Nipane, F. Ali, C. Kim, J. T. Teherani, J. Hone, and W. J. Yoo, 2D Mater. **8**, 012002 (2020).
38) J. Y. Park, H. E. Joe, H. S. Yoon, S. Yoo, T. Kim, K. Kang, B. K. Min, and S. C. Jun, ACS Appl. Mater. Interfaces **9**, 26325 (2017).
39) Y. Hu, G. Li, and Z. Chen, IEEE Electron Device Lett. **39**, 276 (2017).